Pre-curved Beams as Technical Tactile Sensors for Object Shape Recognition

Carsten Behn
Dept. of Mechanical Engineering
Technische Universität Ilmenau
Ilmenau, Germany, 98693
Email: carsten.behn@tu-ilmenau.de

Joachim Steigenberger
Institute of Mathematics
Technische Universität Ilmenau
Ilmenau, Germany, 98693

Anton Sauter and Christoph Will
Dept. of Mechanical Engineering
Technische Universität Ilmenau
Ilmenau, Germany, 98693

***Abstract*—Recent research topics in bionics focus on the analysis and synthesis of animal spatial perception of their environment by means of their tactile sensory organs: vibrissae and their follicles. Using the vibrissae, these mammals (e.g., rats) are able to determine an obstacle shape using only a few contacts of the vibrissa with the object. The investigations lead to the task of creating models and a stringent exploitation of these models in form of analytical and numerical calculations to achieve a better understanding of this sense. The sensing lever element vibrissa for the stimulus transmission is frequently modeled as an Euler-Bernoulli bending rod. We assume that the rod is one-sided clamped and interacts with a rigid obstacle in the plane. But, most of the literature is limited to the research on cylindrical and straight, or tapered and straight rods. The (natural) combination of a cylindrical and pre-curved shape is rarely analyzed. The aim is to determine the obstacles contour by one quasi-static sweep along the obstacle and to figure out the dependence on the pre-curvature of the rod. To do this, we proceed in several steps: At first, we have to determine the support reactions during a sweep. These support reactions are equate with the observables an animal solely relies on and have to be measured by a technical device. Then, the object shape has to be reconstructed in using only these generated observables. The consideration of the pre-curvature makes the analytical treatment a bit harder and results in numerical solutions of the process. But, the analysis of the problem results in an extension of a former decision criterion for the reconstruction by the radius of pre-curvature. Is is possible to determine a formula for the contact point of the rod with the profile, which is new in literature in context of pre-curvature.**

Keywords–Vibrissa; Sensing; Object scanning; Contour reconstruction; Pre-curved beam.

I. INTRODUCTION

In recent years, the development of vibrissae-inspired tactile sensors gain center stage in the focus of research, especially in the field of (autonomous) robotics, see e.g., [1] – [5]. These tactile sensors complement to and/or replace senses like vision, because they provide reliable information (object distance, contour and surface texture) in a dark and noisy environment (e.g., seals detect freshet and turbulence of fish in muddy water [6] [7] [8]), and are cheaper in fabrication.

Most mammals exhibit such vibrissae, in a variety of types and located in various areas of the skin/fur. Vibrissae differ from typical body hairs: they are thicker, longer, embedded in an own visco-elastic support (the so-called "follicle-sinus complex" (FSC)), see also [9] for some illustrations. Moreover, they feature a pre-curvature, a conical shape, cylindrical cross-section and are made of different material with hollow parts (like a multi-layer system) [10] [11] [12]. The vibrissa mainly serves as a force transmission (due to an obstacle contact) to its support. Hence, movement and deformation of the vibrissa can only be detected by mechanoreceptors in the FSC [1] [13]. It is hypothesized, that changing the blood-pressure in the FSC allows the animal to adjust the stiffness of the tissue to control the movement of the vibrissa [10] [12]. Furthermore, the surrounding tissue (fibrous band) and muscles (intrinsic and extrinsic musculature) enable the animal to actively move the vibrissa (active mode for surface texture detection) or to passively return the vibrissa to a rest position after deflection (due to a obstacle contact in passive mode) [14]. The pre-curvature is due to a kind of protection role: purely axial forces are prevented and, including the conical shape, the area of the tip of the vibrissa is limp. This results in a tangential contact to an object [10] [15].

In this paper, the investigations focus the influence of the *pre-curvature* to the static bending behavior of a vibrissa in context of obstacle contour detection and reconstruction. We describe a quasi-static scanning process of obstacles: 1. analytical/numerical generation the observables in the support which an animal solely relies on, 2. reconstruction of the scanned profile contour using only these observables, and 3. verification of the working principle by means of experiments. These steps were done in [5], [16] and [17] for cylindrical vibrissae. Therefore, we extend these results to pre-curved vibrissae in this paper.

The paper is arranged as follows: In Section II, a short overview of the related literature is given. Based on these information, Section III deals with aspects of setting up a mechanical model for the object sensing and presenting the describing equations. These equations are exemplarily solved in Section IV – considering only a constant pre-curvature radius of the bending rod. The results governed by numerical simulations are verified by experiments in Section V. Section VI concludes the paper.

II. SOME STATE OF ART OF PRE-CURVED VIBRISSAE

From the biological point of view, there are a lot of works focussing on the determination of vibrissae parameters. Towal et al. [12] pointed out an important fact that the mostly vibrissae are curved in a plane. The deviation of the vibrissa from this plane (referred to the length) is less than

 ISBN: 978-1-61208-518-0

0.1%. In [12], [15] and [18] – [22], a vibrissa is described using a polynomial approximation of 2nd-, 3rd- and 5th-order, which is rather low. In contrast to this references, we present numerical results using one of order 10. In [15], it is stated that approximately 90% of rat vibrissae exhibit a pre-curvature $\kappa_0 \in (0.0065/mm, 0.074/mm)$, and in [20] that extremely curved vibrissa provide $\kappa_0 > 0.25/mm$. The authors of [11], [15], [20] publish the following dimensionless parameters

$$\frac{L}{d} \approx 30\,, \quad \frac{r_0}{d} \approx 90\,,$$

whereas L is the length, d is the base diameter, and r_0 is the pre-curvature radius of the vibrissa.

From the technical point of view, pre-curved vibrissae are rarely used in applications. In [15], [21], [22], experimental and theoretical investigations concerning the distance detection to a pole are presented, using a pre-curved artificial vibrissa, also incorporating the conical shape. The pros and cons of a positive (curvature forward, CF) and negative (CB) curved vibrissae are stated in [15] whereas the vibrissa is used for tactile sensing of a pole. The CF-scanning results in low axial forces, but higher sheer ones; CB the inverse results. Summarized, the pre-curvature influences mainly the support forces instead of the support moment.

III. MODELING

This section shall serve as an introduction to the profile scanning procedure.

Beam Deflection Formula: The deflection of a largely deformed beam with pre-curvature is described in using the so-called *Winkler-Bach-Theory*. A detailed derivation of the equations can be found in [23] and [24]. Furthermore, the authors in [24] pointed out, that – assuming, that the radius of pre-curvature is much greater than the dimensions of the cross-section – the influence of the normal force can be neglected. Hence, the describing equations can be simplified to

$$\frac{d\varphi(s)}{ds} = \frac{1}{r_0(s)} + \frac{M_{bs}(s)}{E\,I_z}\,, \tag{1}$$

with second moment of area

$$I_z := \int\limits_A \eta^2 dA\,,$$

and Young's modulus E, cross-section A, bending moment M_{bs}, and radius of pre-curvature r_0.

Scanning Procedure: Here, we describe the scanning procedure of *strictly convex profile contours* using pre-curved technical vibrissae *in a plane*. This is done in two steps:

1. Because of analytical interest, we firstly generate the observables (support reactions) during the scanning process. Since our intension is from bionics, we simply model the support as a clamping (being aware that this does not match the reality). Hence, the support reactions are the clamping forces and moment $\vec{M}_{Az}$, $\vec{F}_{Ax}$, $\vec{F}_{Ay}$, which an animal solely relies on.
2. Then, we use these observables in an algorithm to reconstruct the profile contour.

Fig. 1 sketches the scanning process of a plane, strictly profile. For this scanning process, several assumptions are made:

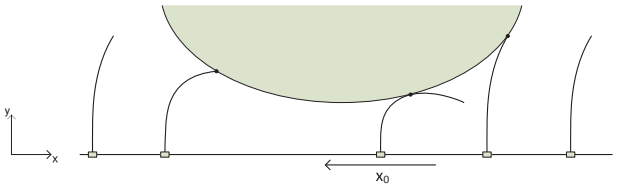

Figure 1. Scanning procedure using an artificial vibrissa; adapted from [5].

- The technical vibrissa is moved from *right to the left* (negative x-direction), i.e., the base point is moved.
- The problem is handled *quasi-statically*, i.e., the vibrissa is moved incrementally (and presented in changes of the boundary conditions). Then, the elastically deformed vibrissa is determined.
- Since we do not want to deal with friction at the beginning, we assume an *ideal contact*, i.e., the contact force is *perpendicular* to the contact point tangent of the profile.

The scanned profile is given by a function $g : x \mapsto g(x)$, where $g \in C^1(\mathbb{R};\mathbb{R})$. Since the graph of g is convex by assumption, the graph can be parameterized by means of the slope angle α in the xy-plane. Then we have, [5]:

$$\begin{aligned} \frac{dg(x)}{dx} &= g'(x) = \tan(\alpha) \\ \longrightarrow x &= \xi(\alpha) := g'^{-1}\big(\tan(\alpha)\big) \\ y &= \eta(\alpha) := g\big(\xi(\alpha)\big) \end{aligned}$$

Therefore, each point of the profile contour is given by $(\xi(\alpha), \eta(\alpha))$, $\alpha \in (-\frac{\pi}{2}, \frac{\pi}{2})$. For generality, we introduce dimensionless variables, starting with the arc length s with $s = Ls^*$, $s^* \in [0,1]$. Then, all lengths are measured in $\mathbf{L}$, all moments in $\mathbf{EI_z L^{-1}}$, and all forces in $\mathbf{EI_z L^{-2}}$, whereby we omit the asterisk "$*$" for brevity from now on.

Boundary-value Problem in Step 1: The system of differential equations (ODEs) describing the deformed pre-curved, technical vibrissa in a plane in dimensionless quantities is:

$$\left.\begin{aligned} \frac{dx(s)}{ds} &= \cos(\varphi(s)) \\ \frac{dy(s)}{ds} &= \sin(\varphi(s)) \\ \frac{d\varphi(s)}{ds} &= \frac{1}{r_{0L}(s)} + f\Big(\big(y(s)-\eta(\alpha)\big)\sin(\alpha) \\ &\qquad +\big(x(s)-\eta(\alpha)\big)\cos(\alpha)\Big) \end{aligned}\right\} \tag{2}$$

Observing Figs. 1 and 2 gives the hint to distinguish two phases of contact between the vibrissa and the obstacle:

- *Phase A – tip contact:* We have still ODE-system (2) with the boundary conditions (BCs)

$$\begin{aligned} y(0) = 0\,, \quad \varphi(0) = \frac{\pi}{2}\,, \\ x(1) = \xi(\alpha)\,, \quad y(1) = \eta(\alpha) \end{aligned} \tag{3}$$

- *Phase B – tangential contact:* Only the BCs change:

$$\begin{aligned} y(0) = 0\,, \quad \varphi(0) = \frac{\pi}{2}\,, \\ x(s_1) = \xi(\alpha)\,, \quad y(s_1) = \eta(\alpha)\,, \quad \varphi(s_1) = \alpha \end{aligned} \tag{4}$$

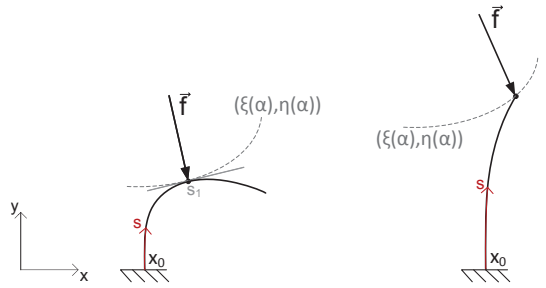

Figure 2. Contact of vibrissa and obstacle in *Phase A* (left) and in *Phase B* (right) during scanning process.

A direct inspection of the occurring problems (2) & (3) and (2) & (4) yield the choice of a shooting method to determine the parameters f and s_1, and finally with f the clamping reactions $\vec{M}_{Az}$, $\vec{F}_{Ax}$, $\vec{F}_{Ay}$.

Initial-value Problem in Step 2: Here, we use only the generated observables (measured in experiments) $\vec{M}_{Az}$, $\vec{F}_{Ax}$, $\vec{F}_{Ay}$ and known base of the vibrissa x_0 to reconstruct the scanned profile. Due to [2], we determine the bending moment, see Fig. 3, to formulate the initial-value problem (IVP) in this step:

$$\left.\begin{aligned} \frac{dx(s)}{ds} &= \cos(\varphi(s)) \\ \frac{dy(s)}{ds} &= \sin(\varphi(s)) \\ \frac{d\varphi(s)}{ds} &= \frac{1}{r_{0L}(s)} - M_{Az} - F_{Ax}y(s) + F_{Ay}\big(x(s) - x_0\big) \end{aligned}\right\} \tag{5}$$

with initial conditions (ICs)

$$x(0) = x_0\,, \quad y(0) = 0\,, \quad \varphi(0) = \frac{\pi}{2} \tag{6}$$

Now, it is necessary – for each input $\{M_{Az}, F_{Ax}, F_{Ay}, x_0\}$

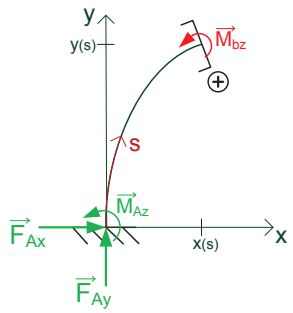

Figure 3. Applying method of sections to the vibrissa.

– to determine the contact point $(x(s_1), y(s_1))$ (note, that s_1 is known in step 1, but is not an observable). But, it is still unknown in which phase we are. We only have

$$M_{bz}(s_1) = 0$$

In accordance to [5], we determine a decision criterion to distinguish both phase. The vibrissa is in Phase B, iff it holds:

$$\boxed{M_{Az}^2 + \frac{2M_{Az}}{r_{0L}} - 2F_{Ay} = 0} \tag{7}$$

In comparison to the condition in [5], we get one new term $\frac{2M_{Az}}{r_{0L}}$. And, in a limiting case for $r_{0L} \longrightarrow \pm\infty$, condition (7) forms the condition in [5], which serves as a validation.

IV. Profile Scanning Using a Constant Pre-curvature Radius

Here, we present numerical simulations of the described profile scanning algorithm (based of two steps). At first, we focus on a *constant* pre-curvature radius $r_{0L} \neq r_{0L}(s)$. Referring to [5], we consider a profile described by $g_1 : x \mapsto \frac{1}{2}x^2 + 0.3$. Exemplarily, two scanning processes are presented in Figs. 4 and 5. Note, that the vibrissae in Phase B are only plotted to the contact point, just for clarity. One can clearly see, that the smaller the pre-curvature radius is no Phase A occurs, i.e., no tip contact, which might explain the protective role of the pre-curvature of vibrissae.

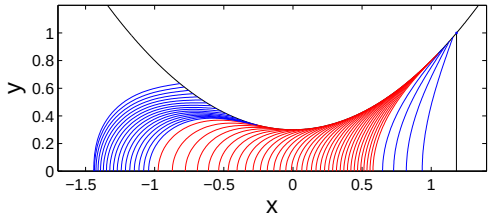

Figure 4. Profile scanning using a pre-curved vibrissa with $r_{0L} = -1000$: in blue *Phase A*, in red *Phase B*.

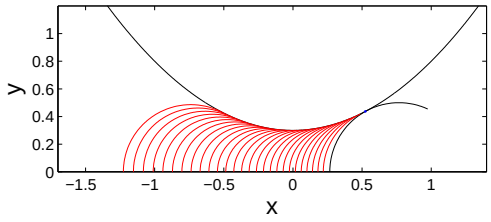

Figure 5. Profile scanning using a pre-curved vibrissa with $r_{0L} = -0.5$: in red *Phase B*, no Phase A.

Figs. 6, 7 and 8 show the observables during a scanning process in dependence on the pre-curvature radius. The transition between both phases is marked with a "+". It becomes clear: the smaller the pre-curvature radius the smaller the bending behavior of the vibrissa, the smaller the observables, but the smaller the scanning area. Therefore, a small pre-curvature radius results in poor scanning results. The error of the reconstruction between the given and reconstructed profile is defined for single points according to [5]:

$$error = \sqrt{\big(x_k(s_{1k}) - \xi(\alpha_k)\big)^2 + \big(y_k(s_{1k}) - \eta(\alpha_k)\big)^2}\,, \tag{8}$$

whereby $(\xi(\alpha_k), \eta(\alpha_k))$ represent a point of the given profile and $(x_k(s_{1k}), y_k(s_{1k}))$ is the corresponding one of the

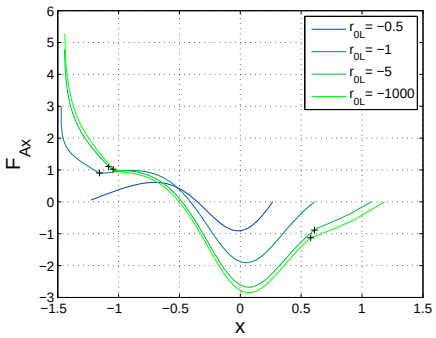

Figure 6. Clamping force F_{Ax} for varying pre-curvature radius r_{0L}.

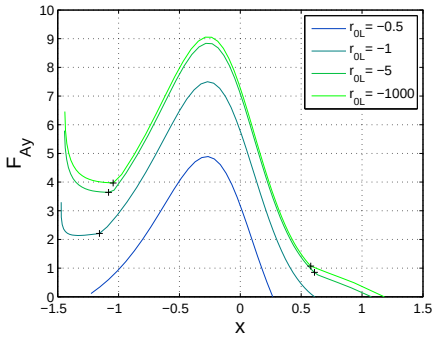

Figure 7. Clamping force F_{Ay} for varying pre-curvature radius r_{0L}.

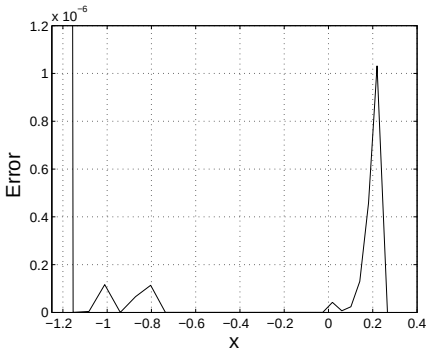

Figure 9. Error of given and reconstructed profile for $r_{0L} = -0.5$.

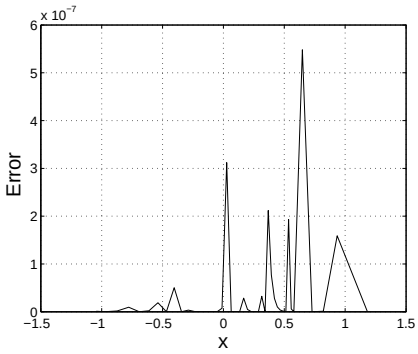

Figure 10. Error of given and reconstructed profile for $r_{0L} = -1000$.

reconstructed profile. Figs. 9 and 10 exemplarily present the reconstruction errors of two reconstruction simulations. The magnitude of the error is from 10^{-7} to 10^{-6}.

V. Experiments in Scanning with Variable Pre-curvature Radius

To verify the algorithms, we present numerical investigations of scanning vibrissae with variable pre-curvature and experimental results, using a parabola profile $g_1(x) = 2x^2 + 0.55$. Three different technical vibrissae with different pre-curvature are used in an experiment. Fig. 11 shows that the first vibrissae is straight, the second and the third one have a variable pre-curvature radius. With the help of a computer-aided evaluation of the graphic representation of the vibrissae in Fig. 11, their pre-curvature radius $r_{0L}(s)$ is determined in dependence of the arc length s as polynomials of order 10. This is rather new in literature, because a lot of works from literature restrict to a representation of the pre-curvature only to s^2-terms.

The simulated scanning processes are shown in Figs. 12 and 13 for vibrissa 1 and 3. Figs. 14, 15 and 16 show exemplarily the observables (simulation vs. experiment) of the experiment using vibrissa 3. An easy inspection confirms prior results, that the maximal values of M_{Az}, F_{Ax} and F_{Ay} decrease the bigger the pre-curvature and the smaller the pre-curvature radius are. These figures show a good coincidence of the simulated and measured curves of the observables.

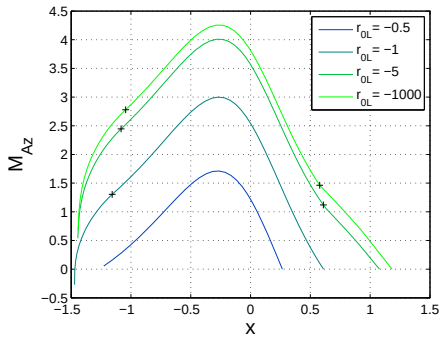

Figure 8. Clamping moment M_{Az} for varying pre-curvature radius r_{0L}.

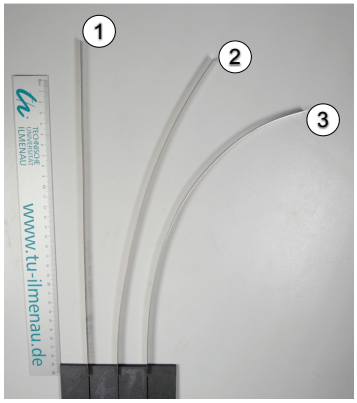

Figure 11. Three different pre-curved vibrissae for the experiment.

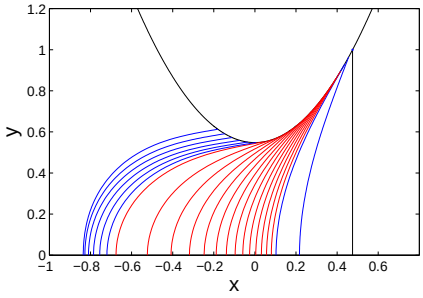

Figure 12. Scanning process using vibrissa 1 – in blue *Phase A*; in red *Phase B*.

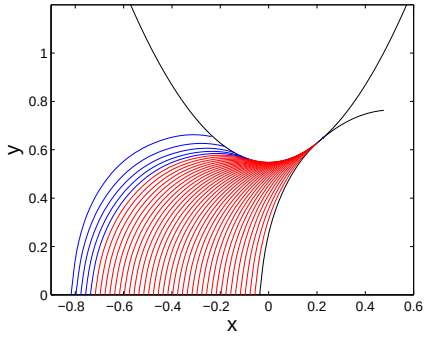

Figure 13. Scanning process using vibrissa 3 – in blue *Phase A*; in red *Phase B*.

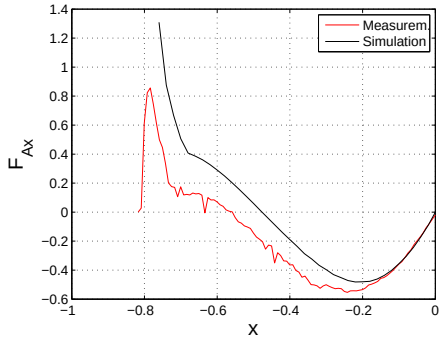

Figure 14. Experiment using vibrissa 3: clamping force F_{Ax} of a simulation and the experiment.

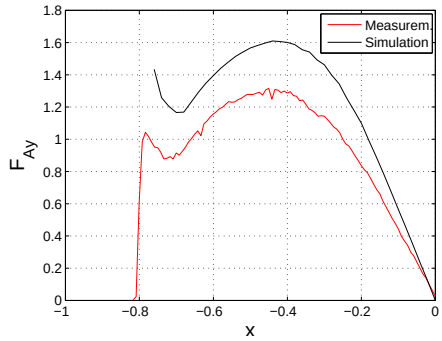

Figure 15. Experiment using vibrissa 3: clamping force F_{Ay} of a simulation and the experiment.

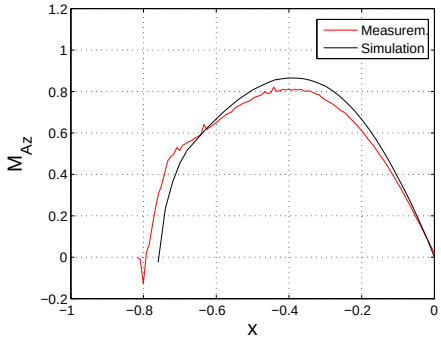

Figure 16. Experiment using vibrissa 3: clamping moment M_{Az} of a simulation and the experiment.

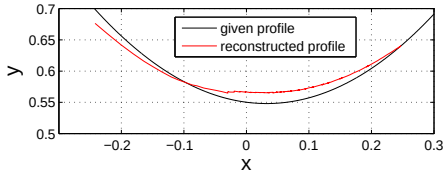

Figure 17. Experiment using vibrissa 3: reconstruction error of a simulation and the experiment.

Fig. 17 presents the reconstruction of the profile. Compared to further simulations, we point out that the smaller the pre-curvature radius is the smaller is the reconstruction error.

Summarizing, we show that it is promising to use pre-curved vibrissae for object contour scanning and reconstruction. The simulated and measured curves of the observables show up a good coincidence. The presented algorithms work effectively.

VI. Conclusion

Due to the functionality of animals vibrissae, the goal was to set up a model for an object scanning and shape reconstruction algorithm. For this, the only available information are the observables (support reaction which an animal solely relies on) governed by one single sweep along the profile. Based on these observables, the object boundary has to be reconstructed. It was possible to illustrate the characteristics and influences of pre-curved technical vibrissae in view of profile scanning. Based on the Winkler-Bach-Theory for pre-curved beams we set up the equations for a deformed vibrissa during a scanning process. We presented an algorithm to reconstruct the scanned profile in using the generated observables (which an animal is supposed to solely rely on) via shooting methods. The reconstruction then was based on solving initial-value problems on contrast to the generation procedure where we solved boundary-value problems. The investigations respective the scanning of a strictly convex profile with a pre-curved vibrissae showed noticeable differences to the profile scanning with a straight vibrissa. The extrema of the bending reactions and the size of the scanned profile area depends on the pre-

 ISBN: 978-1-61208-518-0

curvature radius of the vibrissa. Using a smaller radius, the tangential contact *phase B* in the scanning process could be enlarged. Experiments confirmed the numerical results and algorithms in this paper. Moreover, the investigation showed that the profile reconstruction works better with a pre-curved vibrissa.

ACKNOWLEDGMENT

This work was supported by the Deutsche Forschungsgemeinschaft (DFG), Grant ZI 540-16/2.

REFERENCES

[1] R. Berg and D. Kleinfeld, "Rhythmic Whisking by Rat: Retraction as Well as Protraction of the Vibrissae Is Under Active Muscular Control," Journal of Neurophysiology, vol. 89, no. 1, pp. 104-117, 2002.

[2] G.R. Scholz and C.D. Rahn, "Profile Sensing With an Actuated Whisker," IEEE Transactions on Robotics and Automation, vol. 20, no. 1, pp. 124–127, 2004.

[3] M.J. Pearson et al., "A Biologically Inspired Haptic Sensor Array for use in Mobile Robotic Vehicles," Proceedings of Towards Autonomous Robotic Systems (TAROS), pp. 189-196, 2005.

[4] M.J. Pearson, A.G. Pipe, C. Melhuish, B. Mitchinson, and T.J. Prescott, "Whiskerbot: A Robotic Active Touch System Modeled on the Rat Whisker Sensory System," Adaptive Behavior, vol. 15, no. 3, pp. 223-240, 2007.

[5] C. Will, J. Steigenberger, and C. Behn, "Object Contour Reconstruction using Bio-inspired Sensors," in: Proceedings 11th International Conference on Informatics in Control, Automation and Robotics (ICINCO 2014), September 0103, 2014, Vienna, Austria. IEEE, pp. 459-467, ISBN: 978-989-758-039-0, 2014.

[6] G. Dehnhardt, "Tactile size discrimination by a California sea lion (Zalophus californianus) using its mystacial vibrissae," Journal of Comparative Physiology A, vol. 175, no. 6, pp. 791-800, 1994.

[7] G. Dehnhardt and A. Kaminski, "Sensitivity of the mystacial vibrissae of harbour seals for size differences of actively touched objects," The Journal of Experimental Biology, vol. 198, pp. 2317-2323, 1995.

[8] G. Dehnhardt, B. Mauck, and H. Bleckman, "Seal whiskers detect water movements," Nature, vol. 394, pp. 235-236, 1998.

[9] C. Behn, C. Will, and J. Steigenberger, "Effects of Boundary Damping on Natural Frequencies in Bending Vibrations of Intelligent Vibrissa Tactile Systems," International Journal On Advances in Intelligent Systems, vol. 8, no. 3&4, pp. 245-254, ISSN: 1942-2679, 2015.

[10] K. Carl et al., "Characterization of Statical Properties of Rats Whisker System," IEEE Sensors Journals, vol. 12, no. 2, pp. 340-349, 2012.

[11] D. Voges et al., "Structural Characterization of the Whisker System of the Rat," IEEE Sensors Journals, vol. 12, no. 2, pp. 332-339, 2012.

[12] R.B. Towal, B.W. Quist, V. Gopal, J.H. Solomon, and M.J.Z. Hartmann, "The Morphology of the Rat Vibrissal Array: A Model for Quantifying Spatiotemporal Patterns of Whisker-Object Contact," PLoS Computational Biology, vol. 7, no. 4, pp. 1–17,e1001120, 2011.

[13] A. Ahl, "The role of vibrissae in behavior: A status review," Veterinary Reserarch Communications, vol. 10, pp. 245-268, 1986.

[14] J. Dörfl, "The musculature of the mystacial vobrissae of the white mouse," Journal of Anatomy, vol. 135, no. 1, pp. 147-154, 1982.

[15] B.W. Quist and M.J.Z. Hartmann, "Mechanical signals at the base of a rat vibrissa: the effect of intrinsic vibrissa curvature and implications for tactile exploration," Journal of Neuophysiology, vol. 107, pp. 2298-2312, 2012.

[16] C. Will, J. Steigenberger, and C. Behn, "Quasi-static object scanning using technical vibrissae," in: Proceedings 58. International Colloquium Ilmenau (IWK), September 0812, 2014, Ilmenau, Germany. ilmedia, URL: http://nbn-resolving.org/urn:nbn:de:gbv:ilm1-2014iwk:3 [accessed: 2016-06-10], 2014.

[17] C. Will, J. Steigenberger, and C. Behn, "Bio-inspired Technical Vibrissae for Quasi-static Profile Scanning," Springer International Publishing Switzerland, J. Filipe et al. (eds.), ISBN: 978-3-319-26453-0, pp. 277-295, 2016.

[18] M. Knutsen, D. Derdikman, and E. Ahissar, "Tracking Whisker and Head Movements in Unrestrained Behaving Rodents," Journal of Neurophysiology, vol. 93, pp. 2294-2301, 2004.

[19] M. Knutsen, A. Biess, and E. Ahissar, "Vibrissal Kinematics in 3D: Tight Coupling of Azimuth, Elevation, and Torsion across Different Whisking Modes," Neuron, vol. 59, pp. 35-42, 2008.

[20] N.G. Clack et al., "Automated Tracking of Whiskers in Videos of Head Fixed Rodents," PLoS Computational Biology, vol. 8, no. 7, e1002591, pp. 1–8, 2012.

[21] S.A. Hires, L. Pammer, K. Svoboda, and D. Golomb, "Tapered whiskers are required for active tactile sensation," eLife, 2013, e01350, pp. 1–19, 2013.

[22] L. Pammer et al., "The mechanical variables underlying object lokalisation along the axis of the whisker," The Journal of Neuroscience, vol. 33, no. 16, pp. 6726-6741, 2013

[23] P. Gummert and K.-A. Reckling, "Mechanik (Mechanics)," 3rd edition, Vieweg, Braunschweig, Germany, 1994.

[24] A. Sauter, C. Will, J. Steigenberger, and C. Behn, "Artificial tactile sensors with pre-curvature for object scanning," in: Proceedings 13th Conference on Dynamical Systems – Theory and Applications (DSTA), Lódz, Poland, 7-10 December 2015, Volume "Mathematical and numerical approaches", ISBN: 978-83-7283706-6, pp. 425–436, 2015.

 ISBN: 978-1-61208-518-0